



A new proximate structure for the APB (111) in L1₂ compounds

K.V. Vamsi*, Tresa M. Pollock

Materials Department, University of California Santa Barbara, Santa Barbara, CA 93106, USA

ARTICLE INFO

Article history:

Received 6 December 2019

Revised 19 February 2020

Accepted 21 February 2020

Available online 5 March 2020

Keywords:

Antiphase boundaries

Superalloys

Density functional theory

High-throughput calculations

Planar faults energies

ABSTRACT

A new approach which involves a diffuse multi-layer fault model coupled with a cluster approach to statistical mechanics (CASM) infrastructure has been developed to identify the proximate structure for the antiphase boundary (APB) on {111} planes in L1₂. We report a new structure, 'γ_a' which approximates the bonding environment of an APB better than a previously reported structure, 'ω'. Density functional theory calculations were employed to predict the APB energies from structural energies of γ_a' and L1₂ and were validated against estimations from supercell methods for several binary compounds. The implications of the discovery of the γ_a' are discussed.

© 2020 Acta Materialia Inc. Published by Elsevier Ltd. All rights reserved.

The presence of a coherent, ordered precipitate γ' (L1₂ with A₃B stoichiometry) in many superalloys results in exceptional strength and creep resistance at elevated temperatures [1–3]. Shearing of γ' is reported as one of the dominant deformation mechanisms in aforementioned superalloys over a significant regime of temperature and stress [4–10]. Since the L1₂ precipitates are ordered, the matrix (γ, which is an f.c.c. solid solution) dislocation $\frac{1}{2}[1\bar{1}0]$, is no longer a perfect dislocation and results in the creation of an anti-phase boundary (APB) on the close packed (CP) {111} planes upon shear. As the APB (111) energy increases, the resistance for shearing the precipitates is enhanced, leading to an increase in the overall strength of the alloy. It has been observed that the $\frac{1}{2}[1\bar{1}0]$ dislocations travel in pairs in these two-phase alloys and the peak strength, $\tau_{y,max}$ (Eq. (1)) is observed at the point of transition from a weakly coupled to strongly coupled dislocations shearing mode [11].

$$\tau_{y,max} = 0.81M \frac{\gamma_{APB(111)}}{2b} \left(\frac{3\pi f}{8} \right)^{\frac{1}{2}} \quad (1)$$

where M is the Taylor factor, $\gamma_{APB(111)}$ is the APB energy on the {111} planes, b is the magnitude of the Burgers vector $\frac{1}{2}[1\bar{1}0]$, and f is the volume fraction of γ'. Reed et al. [12] proposed a merit index for strength based on the dependence of strength on APB(111) energy. This index for strength is used to rank alloy compositions for the design of new Ni-base alloy compositions for desired properties [12]. It should be noted that in this method, the estimation

of APB (111) was from a number of Ni₃(Al,X) pseudo-binary compositions using density functional theory (DFT) calculations. The change in APB energy by the substitution of X in Al-sublattice was captured through a coefficient and the synergistic effects arising due to the presence of multiple solute elements were neglected in this method [13].

Recent advances in alloy design in the area of Co-base [14–16] and CoNi-base [17,18] superalloys are largely based on applying the design principles which were developed for Ni-base superalloys and emulating the two-phase microstructure with a high volume fraction of thermodynamically stable coherent L1₂ precipitate. The need for addressing higher order multicomponent systems exists for superalloys as well as “high entropy” or multi-principal element (MPE) alloys where the single-phase alloys may be further strengthened by L1₂ type ordered precipitate [19,20]. Since strength is used as a metric for the alloy design, APB energies in the precipitate phase (refer to Eq. (1)) certainly play an important role in designing two-phase (γ+γ') alloys with better properties in the complex composition spaces. Given the lack of databases on the APB energies for several class of alloys, there is a need for high-throughput methods for estimating the APB energies which can assist the rapid design of these alloys.

Planar fault energies (PFE) are often estimated by ab-initio electronic structure calculations due to the availability of pseudopotentials. These are derived from the structural energies of two supercells (faulted and perfect) with the desired composition over the area of the fault, A (Eq. (2)).

$$\gamma_{PFE} = \frac{E_{faulted} - E_{perfect}}{A} \quad (2)$$

* Corresponding author.

E-mail address: kvvamsi@ucsb.edu (K.V. Vamsi).

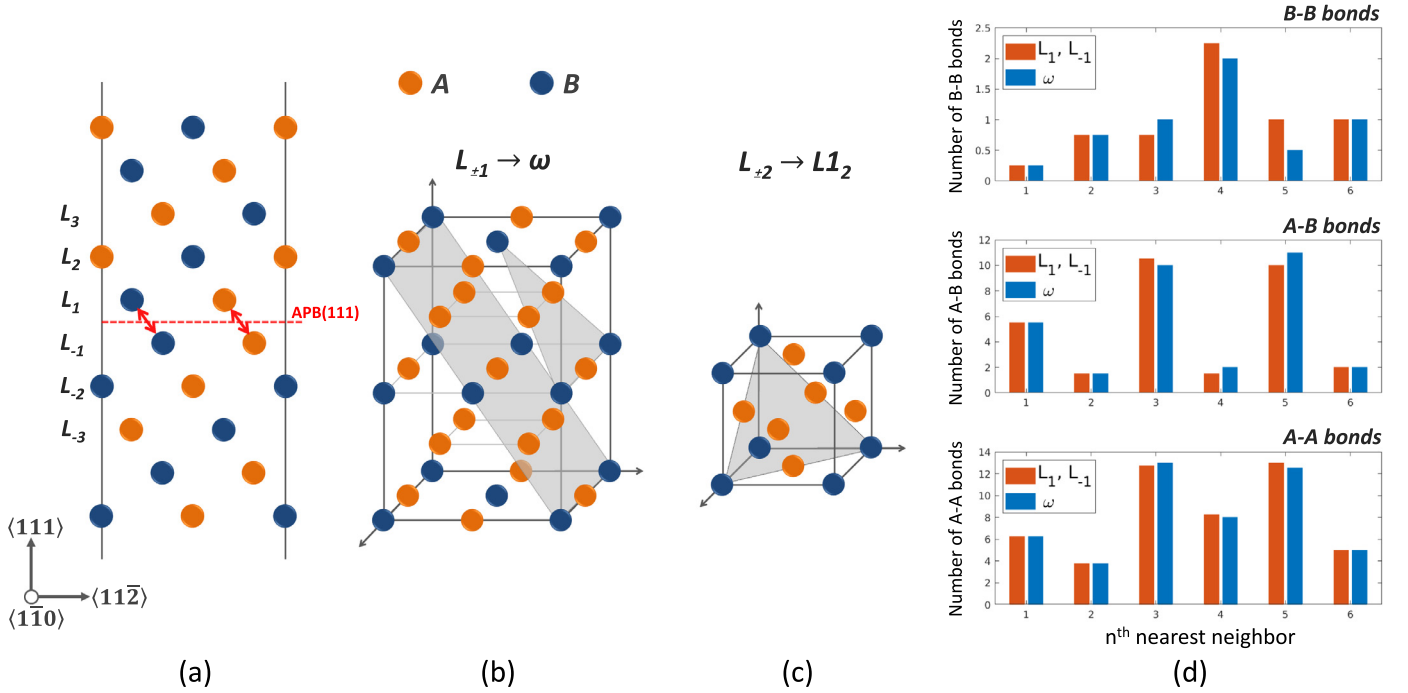


Fig. 1. Schematic showing a) the projection of atoms on a $\langle 110 \rangle$ plane with an APB(111) in an L_{12} , b) the reported proximate structure ' ω ' which approximates layers $L_{\pm 1}$ in an APB(111) [27] c) the proximate structure ' L_{12} ' for layers $L_{\pm 2}$ in an APB(111) [27] and d) comparison of the number of bonds A-A, A-B and B-B at various nearest neighboring distances between $L_{\pm 1}$ and ' ω ' with A_3B stoichiometry.

Since the PFEs are sensitive to the violations across the planar fault, representing the desired composition makes the area of the supercell large, increases the number of configurations to be simulated, thus requiring more computational resources. An alternate method is to approximate the planar fault as a combination of the geometrically close packed (GCP) structures and derive the energies as a function of composition. A one dimensional axial next nearest neighbor Ising (ANNNI) model [21,22] has been used to estimate the planar fault energies in fcc solid solutions [23]. Previously, this methodology has been extended to L_{12} compounds to determine the APB energies and superlattice intrinsic stacking fault (SISF) on the (010) and (111) planes, respectively. It has been shown that the structure of an APB(010) can be approximated by a DO_{22} or DO_{23} structure [24] and SISF(111) can be approximated by a DO_{19} [25,26]. To the best of our knowledge, there is no literature on estimating APB(111) in L_{12} compounds via the ANNNI model and proximate structures corresponding to an APB(111) in L_{12} have not yet been identified.

Recently, a diffuse multi-layer fault (DMLF) model was proposed by Vamsi and Karthikeyan [27] to estimate various planar fault energies in L_{12} structures. In this model, the bonding environment of each layer (L_i) adjacent to the fault is approximated by a respective proximate structure (S_i) which has the same bonding environment of the reference layer and the energy of the faulted structure is expressed as a combination of GCP proximate structures. Therefore, the energy penalty, which is the PFE (in Eq. (2)) can now be expressed as

$$\gamma_{PFE} = \rho \sum_{i=-n}^n [E(L_i) - E(P)] \equiv \rho \sum_{i=-n}^n [E(S_i) - E(P)] \quad (3)$$

Where ρ is the planar density, n is the number of close packed layers, $E(L_i)$, $E(S_i)$ and $E(P)$ are the energies (per atom) of the reference layer, proximate structure and the parent structure.

Fig. 1(a) shows the projection of atoms with an APB(111) on the $\{110\}$ planes in an L_{12} . The atomic planes designated L_1 and L_{-1}

adjacent to the APB have violations (1st nearest neighbor (NN) indicated by arrows) and hence the bonding environment is different compared to the perfect structure. It was found that ' ω ' (Fig. 1(b)) and L_{12} (Fig. 1(c)) are the proximate structures that approximate the bonding environment of layers $L_{\pm 1}$ and $L_{\pm 2}$, respectively [27]. It should be noted that the 'B' atoms on the CP planes take two specific positions in ' ω ' structure. This results in two types of in-plane orderings on the CP planes, a triangular (T) and a rectangular (R) type arrangement alternatively (planes shaded in gray in Fig. 1(b)) while the CP planes, $L_{\pm i}$ parallel to APB(111) have a T-type arrangement of B atoms. Fig. 1(d) shows the comparison of the number of different types of bonds (A-A, A-B, and B-B) between $L_{\pm 1}$ and ' ω '. The deviations in the bonding arise from 3rd NN and so on which manifest as an error in estimating the APB energies. The objective of this work is to carry out the proximate structure search on a large library of structures and report the discovery of a new structure relevant to an APB (111).

The introduction of a planar fault can disrupt the local stacking and chemical environment in the vicinity of the faults which contribute to the PFE. Therefore, proximate structures that capture these local changes are useful for calculating fault energies. In the DMLF model, it was proposed that there are two steps involved in identifying these proximate structures: 1) Identification of stacking environment of atoms in L_i and 2) Identification of chemical environment of atoms in L_i . The first exercise is to identify the subset of structures with same stacking environment of atoms on L_i . Since creation of an APB does not change the stacking environment, the possible proximate structures S_i for various layers L_i should also possess the stacking sequence ...|ABC|... akin to f.c.c. The next step is to find the proximate structure S_i , which mimics the chemical environment of L_i from a set of structures ' H '. A specific structure $H_q \in H$ can be represented by a unique coordinate in a ' $3n$ ' dimensional bond count space (factor 3 arises due to three types of bonds A-A, A-B and B-B in binary A_3B compound). This coordinate consists of a set of numbers which are the bond counts at different NN distances for the structure H_q , which can be expressed as

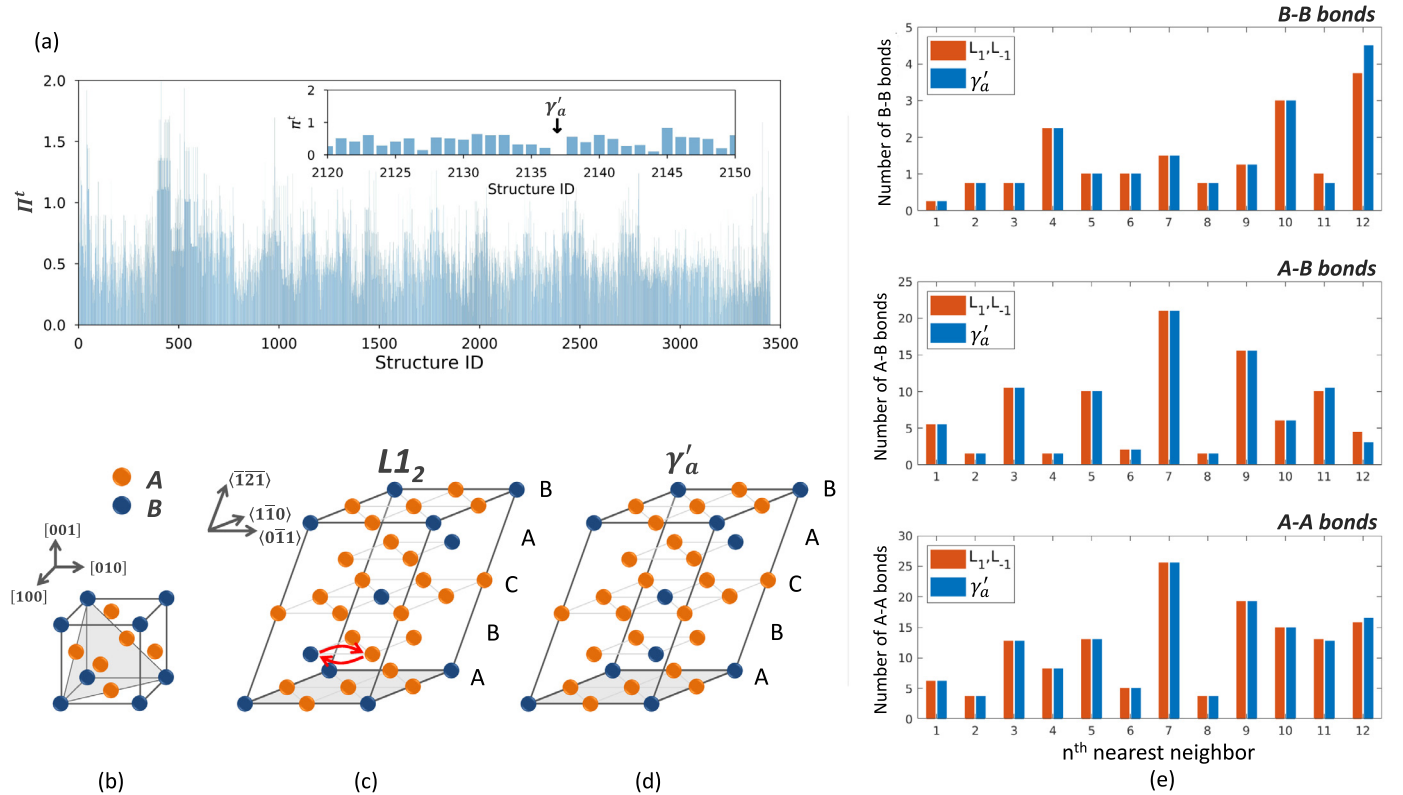


Fig. 2. (a) The proximity Π^t , evaluated between L_1 in APB(111) and the structures S_i (orderings in f.c.c.). The inset shows the corresponding proximate structure γ'_a for L_1 which has the minimum Π^t . (b) L_{12} with basis vectors as b) $[100]$, $[010]$ and $[001]$, c) $\langle 011 \rangle$, $\langle 1\bar{1}0 \rangle$ and $\langle \bar{1}2\bar{1} \rangle$ and d) comparison of the number of bonds A-A, A-B and B-B at various nearest neighboring distances between $L_{\pm 1}$ and γ'_a with A_3B stoichiometry.

$(N_1^{AA,H_q}, N_1^{AB,H_q}, N_1^{BB,H_q}, N_2^{AA,H_q}, N_2^{AB,H_q}, N_2^{BB,H_q}, \dots, N_n^{AA,H_q}, N_n^{AB,H_q}, N_n^{BB,H_q})$ where N_1^{AA,H_q} is the number of A-A bonds at 1st NN distance. Similarly, bonding environment of L_i can be uniquely expressed as $(N_1^{AA,L_i}, N_1^{AB,L_i}, N_1^{BB,L_i}, N_2^{AA,L_i}, N_2^{AB,L_i}, N_2^{BB,L_i}, \dots, N_n^{AA,L_i}, N_n^{AB,L_i}, N_n^{BB,L_i})$. Now, the proximity Π^t , is defined as the norm of the vector connecting the two points L_i and H_q in the $3n$ dimensional bond count space as:

$$\Pi^t(L_i, H_q) = \sqrt{\sum_{j=1}^n w_j^2 \left\{ (\Delta N_j^{AA}(L_i, H_q))^2 + (\Delta N_j^{AB}(L_i, H_q))^2 + (\Delta N_j^{BB}(L_i, H_q))^2 \right\}} \quad (4)$$

where $\Delta N_j^{AA}(L_i, H_q) = N_j^{AA,H_q} - N_j^{AA,L_i}$, w_j is the weighting factor at the j th NN distance and $w_1 > w_2 > \dots > w_j$. These weights are derived from the Morse interatomic potential of Ni [28] and the relative weights scale with the bond strength at each NN distance (w_j used in this work are provided in the supplementary material). If the value of Π^t in Eq. (4) is zero, it suggests that the structure H_q and the reference structure L_i have identical bonding environments. Other values of Π^t capture the deviation of bonding environment of H_q from the reference structure L_i .

Using the enumeration module implemented in the software ‘CASM: Cluster approach to statistical mechanics’ [29–32], a library of about 3450 structures (orderings in fcc, ≤ 16 atoms, A_3B stoichiometry) was generated for the proximate structure search. Π^t was evaluated, using data up to 10th NN distance, for the layer L_1 , within the APB (111) as the reference structure (refer Fig. 1(a)). The structure which yields the minimum Π^t was identified as the

proximate structure S_1 for L_1 . Fig. 2(a) shows that estimated values of Π^t over all the structures with reference layer as L_1 . Interestingly, there exists a structure which has a Π^t value of zero (inset in Fig. 2(a)) suggesting an exact match between the bonding environment of the proximate structure and the reference layer L_1 . This new GCP structure from here on will be referred as “ γ'_a ” (crystallographic details and a sample POSCAR file is presented in the supplementary material). The primitive cell of γ'_a (shown in Fig. 2(d)) has 16 atoms with A_3B stoichiometry. In γ'_a , the B-type atoms (shaded in blue) on every CP plane are arranged in a T-type configuration like that of an L_{12} structure (the CP plane is shaded in gray, refer to Fig. 2(b)). Moreover, the structures of γ'_a and L_{12} are closely related. The L_{12} can be transformed into an γ'_a by a simple exchange of a B-type atom with an A-type atom on one of the closed packed planes in L_{12} (with supercell shape of γ'_a) as shown in Fig. 2c (swap indicated by arrows in red).

The comparison of bond counts between the two bonding environments, $L_{\pm 1}$ and γ'_a are shown in Fig. 2(e). It should be noted that the match in the bond counts (A-A, A-B, and B-B) between $L_{\pm 1}$ and γ'_a exists up to 10th NN distance ($\sqrt{5}a$, where ‘ a ’ is lattice parameter if A_3B in L_{12}) while the previously reported relevant structure ‘ ω ’ has a match only up to the first two neighboring distance with reference structure L_1 . A similar analysis was carried out for other layers in APB (111). It was found that reference layers L_2 , L_3 and so on are better represented by L_{12} as reported previously [27]. Now that a new structure is found which approximates APB (111), the energy can be expressed in terms of structural energies via the DMLF model as:

$$\gamma_{APB(111)} = 2\rho_{(111)}(E_{\gamma'_a} - E_{L_{12}}) \quad (5)$$

where $\rho_{(111)}$ is the planar density of the CP planes, $E_{\gamma'_a}$ and $E_{L_{12}}$ are the structural energies of γ'_a and L_{12} structures respectively.

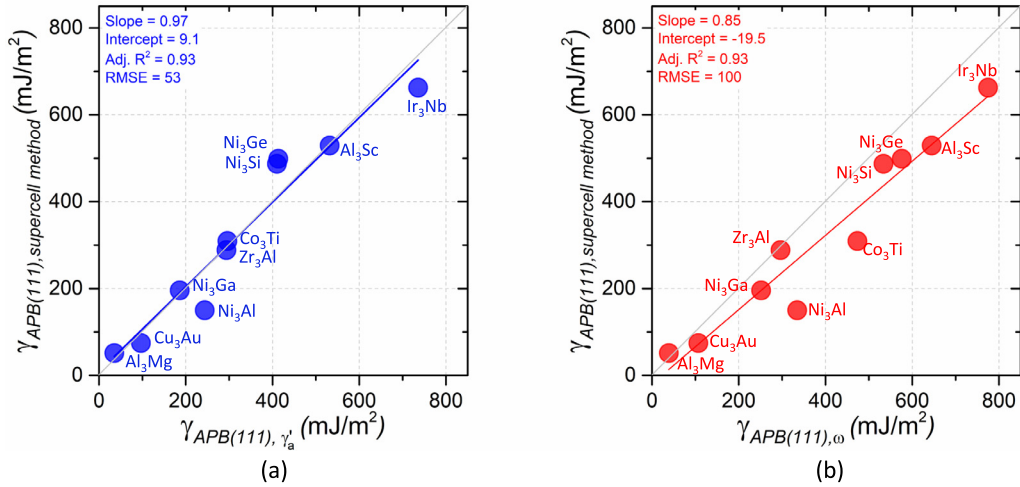


Fig. 3. $\gamma_{APB(111)}$ predicted by the DMLF model using a) γ'_a and b) ω' compared against results from supercell method over a variety of stable L_{12} compounds (slope, Intercept, Adj. R^2 and RMSE (in mJ/m^2) for the best fit is also indicated).

The factor of ‘2’ arises because both the layers, L_{-1} and L_1 are represented by γ'_a .

To validate the γ'_a structure, APB (111) energies in several A_3B compounds were estimated in two different ways: a) supercell method and b) DMLF model. For the first set of calculations, the energies were estimated using the expression in Eq. (2). The planar fault of interest is APB(111) and the modified expression is given by $\gamma_{APB(111), \text{supercell}} = \frac{E_{APB(111)} - E_{L_{12}}}{A}$. $E_{L_{12}}$ was obtained by constructing a supercell with $[1\bar{1}0]$, $[0\bar{1}1]$ and $[111]$ as the basis vectors (12 $\{111\}$ type layers, with 4 atoms on each layer). $E_{APB(111)}$ was estimated by creating an APB (111) in the supercell using a tiling technique [33,34] where the atomic positions were fixed with respect to the original supercell, but the basis vectors of the supercell were chosen such that the two blocks of the crystal are sheared with respect to each other by the corresponding shear vector and a planar fault is created upon imposing periodic boundary conditions. The size of the supercell was chosen such that there are no interactions between the periodic images of APBs [35]. The second set of calculations involved estimating APB energies from the structural energies in L_{12} (4 atoms) and γ'_a (16 atoms) (using Eq. (5)). The Vienna Ab-initio simulation package (VASP) was used to perform the DFT simulations [36]. Pseudopotentials based on the generalized gradient approximation (GGA) [37] and Methfessel-Paxton distribution with a smearing width of 0.2 eV was used [38]. A k -point mesh of $15 \times 15 \times 15$ was used for the unit cells in L_{12} . While the dimension of γ'_a and supercells (with and without fault) were constrained to L_{12} dimensions, atomic relaxation is allowed until the forces on individual atoms is less than 0.02 eV/Å. A plane wave cut-off of 550 eV was used. All the calculations were spin-polarized. The system size was between 4 and 48 atoms and calculations were performed for several A_3B compounds that are stable in L_{12} .

Fig. 3(a) shows the comparison of $\gamma_{APB(111)}$ predicted from DMLF model against the traditional supercell method ($\gamma_{APB(111), \text{supercell}}$). Interestingly, all the data falls closer to the unity line with the following fit parameters: slope = 0.97, $R^2 \sim 0.93$, $\text{RMSE} = 53 \text{ mJ}/\text{m}^2$, where $\text{RMSE} = \sqrt{\frac{\sum_{i=1}^n (\gamma_{\text{direct},i} - \gamma_{\text{DMLF},i})^2}{n}}$. The $\gamma_{APB(111)}$ estimations from the supercell method were expected to be higher than the estimations from DMLF model because of the γ'_a structure accounts for the energy contributions only from layer L_1 in the APB(111). It was found that the atomic relaxations in the vicinity of APB(111) resulted in a greater reduction of $\gamma_{APB(111)}$ in the supercells compared to a reduction in energy of

γ'_a (refer to Fig. S1 in the supplementary document). The energy contributions from layer L_2 to the APB(111) are elegantly compensated by a greater reduction of $\gamma_{APB(111)}$ in the supercells and this is manifested as a slope of 0.97 (close to unity). Fig. 3(b) shows a comparison between $\gamma_{APB(111)}$ predicted with ω' as the proximate structure and $\gamma_{APB(111), \text{supercell}}$ (slope ~ 0.85 , $R^2 \sim 0.93$, $\text{RMSE} = 100 \text{ mJ}/\text{m}^2$). The results in Fig. 3 validate that APB (111) is better represented by an γ'_a compared to ω' . Though there is some correlation in the predictions with values from direct simulations, ω' overestimates the APB (111) energies. Clearly, ω' does not completely approximate the APB (111) (refer to Fig. 1(d)), due to deviations in the bonding environment. Another possible reason for this observation is that the ordering of B atoms within ω' is such that the B atoms (shaded in blue, refer Fig. 1b) were arranged as a column in one of the CP directions. Such an arrangement restricts the atomic relaxations of B atoms along that direction. The bond length of a B-B type bond after relaxation is much lower (magnitude is the same as a first nearest neighbor distance in perfect L_{12}) in a ω' compared to a B-B bond across the APB(111) (refer Fig. S2). The strain energy in the ω' also adds up to the estimation of $\gamma_{APB(111)}$. It should also be mentioned that the magnitude of atomic relaxation in these structures and the reduction of APB(111) energies certainly depend on the atomic species in the compound. Thus in the nearest neighbor bond model, the structure of an APB(111) is better approximated by an γ'_a compared to ω' . It should be highlighted that the structures γ'_a and ω' have the same number of atoms in the unit cell, hence the computational advantage of the DMLF approach over direct methods will remain the same (~ 15 -fold for binaries).

High-throughput estimations of $\gamma_{APB(111)}$ in model pseudo-binary compositions including $\text{Ni}_3\text{Al}_{0.75}\text{Ta}_{0.25}$, $\text{Ni}_3\text{Al}_{0.5}\text{Ti}_{0.5}$, $\text{Co}_3\text{Al}_{0.5}\text{W}_{0.5}$, and $\text{Co}_3\text{Ti}_{0.55}\text{Cr}_{0.45}$ [39–41] which are simplified compositions in γ' were chosen for further study. The structural energies for representative compositions in L_{12} (8 atoms in supercell) and γ'_a (16 atoms in supercell) are shown in Table 1. Average structural energies (using a Boltzmann averaging) were obtained for each composition and the $\gamma_{APB(111)}$ energies were estimated using Eq. (5). Table 1 also shows the comparison between the $\gamma_{APB(111)}$ energies predicted via the DMLF model and the values estimated by supercell methods reported in prior research [13,34,42–45]. It can be observed that there is a variation in $\gamma_{APB(111)}$ energies reported in the literature and that the values estimated from the proximate γ'_a structure fall within the reported range. Interestingly, Ni-based compositions possess higher APB

Table 1

$\gamma_{APB(111)}$ energies in a few model pseudo-binary compounds predicted via DMLF model (using γ'_a) and comparison of the data reported in the literature [13,34,42–45].

Compound	$\gamma_{APB(111)}$ (in mJ/m ²)	
	Present study	Literature (supercell method)
Ni ₃ Al _{0.75} Ta _{0.25}	452	372 [42], 612 [43]
Ni ₃ Al _{0.5} Ti _{0.5}	468	383 [42], 500 [13], 633 [43]
Co ₃ Al _{0.5} W _{0.5}	358	271 [34], 193 [44], 389 [45]
Co ₃ Ti _{0.5} Cr _{0.5}	393	–

energies compared to the Co-based compositions. This analysis also demonstrates that the DMLF methodology can be used to predict APB energies in a high-throughput manner. The DMLF model coupled with cluster expansion techniques can provide the configurational entropy contributions to the free energies that can inform thermodynamic databases such as those by ThermoCalc [46] and can directly benefit the alloy design process.

In conclusion, a new methodology for assessing APB energies has been demonstrated. The DMLF model coupled with a large database of enumerations with A₃B stoichiometry in the CASM infrastructure was used to discover a new hypothetical structure γ'_a which provides an improved approximation of the bonding environment of APB(111) compared to the previously reported ω [27]. DFT calculations were performed to estimate APB(111) energies from structural energies of the γ'_a and L1₂ and these predictions were validated against values derived from traditional supercell methods. In addition to the phase stability, peak strength (Eq. (1)) can also be used as an additional design parameter which can expedite the design process for desired mechanical properties.

Declaration of Competing Interest

The authors declare that they have no known competing financial interests or personal relationships that could have appeared to influence the work reported in this paper.

Acknowledgments

The authors acknowledge the support of DoD Vannevar Bush Fellowship, ONR Grant N00014-18-1-3031. We thank Prof. Anton Van den Ven, Mr. N. S. Harsha Gunda and Mr. Sanjeev Krishna Kolli for useful discussions and assistance with the CASM software.

Supplementary materials

Supplementary material associated with this article can be found, in the online version, at doi:10.1016/j.scriptamat.2020.02.038.

References

- [1] J.H. Westbrook, Elsevier, 1996, pp. 1–26.
- [2] D. Caillard, A. Couret, Elsevier, 1996, pp. 69–134.
- [3] T.M. Pollock, R.D. Field, Elsevier, 2002, pp. 547–618.
- [4] C. Carry, J.L. Strudel, Acta Metall. 26 (1978) 859–870.
- [5] N. Matan, D.C. Cox, C.M.F. Rae, R.C. Reed, Acta Mater. 47 (1999) 2031–2045.
- [6] J.X. Zhang, T. Murakumo, H. Harada, Y. Koizumi, Scr. Mater. 48 (2003) 287–293.
- [7] A. Sato, A.-C. Yeh, T. Kobayashi, T. Yokokawa, H. Harada, T. Murakumo, J.X. Zhang, Energy Mater. 2 (2007) 19–25.
- [8] C.M.F. Rae, R.C. Reed, Acta Mater. 55 (2007) 1067–1081.
- [9] D.M. Knowles, Q.Z. Chen, Mater. Sci. Eng. A 340 (2003) 88–102.
- [10] L. Kovarik, R.R. Unocic, J. Li, P. Sarosi, C. Shen, Y. Wang, M.J. Mills, Prog. Mater. Sci. 54 (2009) 839–873.
- [11] A.J. Ardell, Metall. Trans. A 16 (1985) 2131–2165.
- [12] R.C. Reed, A. Mottura, D.J. Crudden, in: Superalloys, John Wiley & Sons, Ltd., 2016, pp. 13–23.
- [13] D.J. Crudden, A. Mottura, N. Warnken, B. Raeisnia, R.C. Reed, Acta Mater. 75 (2014) 356–370.
- [14] A. Suzuki, H. Inui, T.M. Pollock, Annu. Rev. Mater. Res. 45 (2015) 345–368.
- [15] T.M. Pollock, J. Dibbern, M. Tsunekane, J. Zhu, A. Suzuki, JOM 62 (2010) 58–63.
- [16] A. Suzuki, T.M. Pollock, Acta Mater. 56 (2008) 1288–1297.
- [17] M.S. Titus, Y.M. Eggeler, A. Suzuki, T.M. Pollock, Acta Mater. 82 (2015) 530–539.
- [18] M.S. Titus, High Temperature Deformation Mechanisms of L1₂-Containing Co-Based Superalloys PhD Thesis, University of California Santa Barbara, 2015.
- [19] S. Haas, A.M. Manzoni, F. Krieg, U. Glatzel, Entropy 21 (2019) 169.
- [20] T. Yang, Y. Zhao, W. Liu, J. Kai, C. Liu, J. Mater. Res. 33 (2018) 2983–2997.
- [21] P.J.H. Denteneer, W. van Haeringen, J. Phys. C Solid State Phys. 20 (1987) L883.
- [22] C. Colinet, A. Pasturel, Philos. Mag. Part B 82 (2002) 1715–1729.
- [23] L. Vitos, J.-O. Nilsson, B. Johansson, Acta Mater. 54 (2006) 3821–3826.
- [24] C. Colinet, A. Pasturel, Intermetallics 10 (2002) 751–764.
- [25] A. Mottura, A. Janotti, T.M. Pollock, Intermetallics 28 (2012) 138–143.
- [26] A. Breidi, J. Allen, A. Mottura, Phys. Status Solidi B (2017) 254.
- [27] K.V. Vamsi, S. Karthikeyan, Acta Mater. 145 (2018) 532–542.
- [28] L.A. Girifalco, V.G. Weizer, Phys. Rev. 114 (1959) 687–690.
- [29] J.C. Thomas, A.V. der Ven, Phys. Rev. B 88 (2013) 214111.
- [30] B. Puchala, A. Van der Ven, Phys. Rev. B 88 (2013) 094108.
- [31] A. Van der Ven, J.C. Thomas, Q. Xu, J. Bhattacharya, Math. Comput. Simul. 80 (2010) 1393–1410.
- [32] CASM Developers, CASMcode: v0.2.1, 2017.
- [33] K.V. Vamsi, S. Karthikeyan, in: MATEC Web Conf. 14, 2014, p. 11005.
- [34] K.V. Vamsi, S. Karthikeyan, Scr. Mater. 130 (2017) 269–273.
- [35] Y. Rao, T.M. Smith, M.J. Mills, M. Ghazisaeidi, Acta Mater. 148 (2018) 173–184.
- [36] G. Kresse, J. Furthmüller, Phys. Rev. B 54 (1996) 11169–11186.
- [37] J.P. Perdew, K. Burke, M. Ernzerhof, Phys. Rev. Lett. 77 (1996) 3865–3868.
- [38] M. Methfessel, A.T. Paxton, Phys. Rev. B 40 (1989) 3616–3621.
- [39] K. Muraleedharan, R. Balamuralikrishnan, N. Das, J. Mater. Sci. 44 (2008) 2218–2225.
- [40] J.Y. Hwang, R. Banerjee, J. Tiley, R. Srinivasan, G.B. Viswanathan, H.L. Fraser, Metall. Mater. Trans. A 40 (2009) 24–35.
- [41] N.L. Okamoto, T. Ohashi, H. Adachi, K. Kishida, H. Inui, P. Veyssi re, Philos. Mag. 91 (2011) 3667–3684.
- [42] K.V. Vamsi, Planar Fault Energies in L1₂ Compounds PhD Thesis, Indian Institute of Science, 2018.
- [43] M. Chandran, S.K. Sondhi, Model. Simul. Mater. Sci. Eng. 19 (2011) 025008.
- [44] J.E. Saal, C. Wolverton, Acta Mater. 103 (2016) 57–62.
- [45] L. Feng, D. Lv, R.K. Rhein, J.G. Goiri, M.S. Titus, A. Van der Ven, T.M. Pollock, Y. Wang, Acta Mater. 161 (2018) 99–109.
- [46] J.-O. Andersson, T. Helander, L. H glund, P. Shi, B. Sundman, Calphad 26 (2002) 273–312.